

Development of fragility curves by incorporating new spectral shape indicators and a weighted damage index: case study of steel braced frames in the city of Mashhad, Iran

Hamid Kazemi^{1†}, Mohsen Ghafory-Ashtiany^{2*} and Alireza Azarbakht^{3§}

1. *Department of Civil Engineering, Science and Research Branch, Islamic Azad University, Tehran, Iran*

2. *International Institute of Earthquake Engineering and Seismology (IIEES), Tehran, Iran*

3. *Department of Civil Engineering, Faculty of Engineering, Arak University, Arak, Iran*

Abstract: In this study, strong ground motion record (SGMR) selection based on Eta (η) as a spectral shape indicator has been investigated as applied to steel braced frame structures. A probabilistic seismic hazard disaggregation analysis for the definition of the target Epsilon (ϵ) and the target Eta (η) values at different hazard levels is presented, taking into account appropriately selected SGMR's. Fragility curves are developed for different limit states corresponding to three representative models of typical steel braced frames having significant irregularities in plan, by means of a weighted damage index. The results show that spectral shape indicators have an important effect on the predicted median structural capacities, and also that the parameter η is a more robust predictor of damage than searching for records with appropriate ϵ values.

Keywords: vulnerability; spectral shape indicator; incremental dynamic analysis; damage index; hazard disaggregation; record selection

1 Introduction

In order to prepare a reliable seismic risk analysis of an area, a well-thought out seismic hazard modelling system has to be defined, with good knowledge and data about the elements at risk. This can be done by means of appropriate fragility curves for seismic vulnerability evaluation.

According to the source of the statistical damage data selected, which is used for fragility curve generation, four different types of generic curve types exist: (1) empirical curves; (2) judgment curves; (3) analytical curves, and (4) hybrid curves. Empirical curves, which are based on observed earthquake damage data, are the most reliable. However, in the absence of sufficient data about damage, and particularly in the case of engineered buildings as well as other newer buildings (designed based on latest codes), analytical seismic fragility can be a suitable method of analysis, especially when enough information is available about the structural characteristics of such buildings, as well as about their probable seismic behavior.

Correspondence to: Hamid Kazemi, Department of Civil Engineering, Science and Research Branch, Islamic Azad University, Tehran, Iran
Tel: +982144845144
E-mail: hamid.kazemi@srbiau.ac.ir

[†]PhD Candidate; ^{*}Professor; [§]Assistant Professor

Received June 11, 2015; Accepted November 7, 2015

Analytical seismic fragility is usually calculated from the results of a disaggregation analysis, the selection of representative structures being based on their taxonomy, structural analysis, damage criteria, and probability distribution functions (e.g. a lognormal function). This study, however, is focused on ground motion records selection for structural analysis and damage criteria.

When performing structural collapse assessments, current code-based practice is usually conservatively biased. A different method for the more reliable estimation of damage is therefore required, which could be adapted to local building construction systems, and could vary from area to area. In this way, spectral shape characteristics and damage criteria could be used for structural collapse assessment. Taking into account the fact that, in incremental dynamic analysis (IDA), careful strong ground motion record (SGMR) selection can reduce the bias and variance of the structural response, advanced intensity measures (IM) were used in the analyses presented herein.

In the past, time-domain peak parameters, such as peak ground response parameters (PGA, PGV or PGD), and spectral response parameters (S_a , S_v or S_d) have been the most common scalar IMs. In recent years, vector-valued IMs have been proposed which could increase the efficiency and sufficiency of IMs. It was shown that some of these parameters, which have little effect on the structural response when considered alone as an IM, can perform better when combined with a second IM in

a vector-valued IM (Bojórquez *et al.*, 2012; Gehl *et al.*, 2013; Yakhchalian *et al.*, 2014, 2015). Also, many more reasonable IM (spectral acceleration averaged over a period range) have been proposed based on the fact that higher-order vibration modes play an important role in seismic response (Baker and Cornell, 2006; Lu *et al.*, 2013; Eads *et al.*, 2015).

Many researchers were of the opinion that the selection of ground motion parameters, along with a good structural specification, can be more effective for IMs. Previous studies have shown that Epsilon (ϵ), as a spectral shape indicator, is a good parameter for the reduction of bias, and is more effective than searching for records with appropriate magnitude (M) and source-to-site distance (R) (Baker and Cornell, 2006, Goulet *et al.*, 2006). Apart from this, the parameter Eta (η) (Mousavi *et al.*, 2011; Azarbakht *et al.*, 2015), which takes into account a linear combination of ϵ_{S_a} and the peak ground velocity Epsilon (ϵ_{PGV}), and is more efficient than the well-known and convenient ϵ_{S_a} , has been used as a new IM for the development of fragility curves (which can lead to a reduction in the number of dynamic analyses required to estimate response with a given precision). Using the Eta indicator, it is possible to enhance other response predictors.

On the other hand, when estimating the likely damage to buildings, an appropriate damage assessment method must be defined if reliable fragility curves are to be obtained. Various local, global, cumulative and non-cumulative damage indices have been proposed by different authors for the evaluation of existing buildings. Different criteria, e.g. drifts, accelerations, fatigue, or energy indices, have also been suggested (Williams and Sexsmith, 1995; Ghobarah *et al.*, 1999; Estekanchi and Arjomandi, 2007). Although most of the proposed indices have been applied mainly to concrete structures, some, based on ductility or dissipated energy, have been proposed specifically for steel structures (Khashaee, 2005; Benavent-Climent, 2007; Gerami *et al.*, 2013).

Note that a damage index should be able to reflect features such as torsion and bi-directional response in the case of irregular structures. The damage calculation method proposed by Jeong and Elnashai (2006) was used for the analysis of a typical multi-story, irregular-in-plan building, and a modified damage calculation method was developed for use in the case of three multi-storied irregular buildings, using weighted damage indices.

This study is first, focused on the development of fragility curves for the most commonly found buildings in the city of Mashhad, which is the second largest city in Iran, for S_a as a typical IM, as well as for ϵ or η as special IMs. IDA was performed using the OpenSees platform for a set of SGMR's that were based on both ϵ_{S_a} -filtration and η -filtration procedures. Since the advantages of applying advanced IMs are (1) sufficiency; (2) efficiency, and (3) scaling robustness, the effects of two spectral shape indicators (ϵ and η) were investigated. Three structural limit states (i.e. Immediate Occupancy

(IO), Life Safety (LS) and Collapse Prevention (CP)) were defined for each IDA curve, and the corresponding damage measures were estimated. Finally, the proposed method takes into account the multi-story character of the building, as well as its asymmetry and the probable multi-directionality of earthquake motions. Variability of the fragility curves is considered using record-to-record and modelling uncertainties, using the first-order-second-moment (FOSM) method, and the corresponding probability of damage has been obtained for 72, 475 and 2475 year return periods.

2 Structural modelling

Performance based earthquake engineering (PBEE) requires that structures perform safely in the case of the frequent as well as less frequent ground motions, which are those that mostly contribute to damage, financial loss and the risk of collapse. In order to predict the inelastic response of these structural systems under seismic loads, structural parameters such as the geometrical dimensions of the building, the strength of the materials used, the yield behavior in tension and compression, strain hardening and stiffening phenomena deterioration in the case of large deformations of buildings, need to be accurately simulated. Thus, if more reliable results are to be obtained, all of the above-mentioned properties have to be carefully taken into consideration.

2.1 Selection of buildings

Since conventional Steel X-Braced frames (CBF) constitute approximately 50% of all buildings constructed in Mashhad city during the past two decades (according to the available census data for the Municipality of Mashhad, 2012), this study is focused on the most conventional types of existing buildings, and based on the results of a comprehensive survey, as shown in Fig. 1. In the case of other types of design, further studies will be needed in the future. Thus, three to five-story residential buildings were selected, which were designed according to the Iranian Code of Practice for Seismic Resistant Design of Buildings (Standard No. 2800, 2st edition, 1999) and were built between 2000 to 2006. Figure 1 shows the three representative models in plan view. Also, the specifications of the three selected buildings are presented in Table 1, and a detailed table showing the characteristic sections of the three selected buildings is presented in Table 2.

2.2 Material properties

The material properties of the selected buildings were defined based on the results of past experimental studies. Considering the fact that few tests of entire braced-frame systems have been performed, especially ones incorporating details representative of the current practice in Iran (Shirian, 2005), the results of component

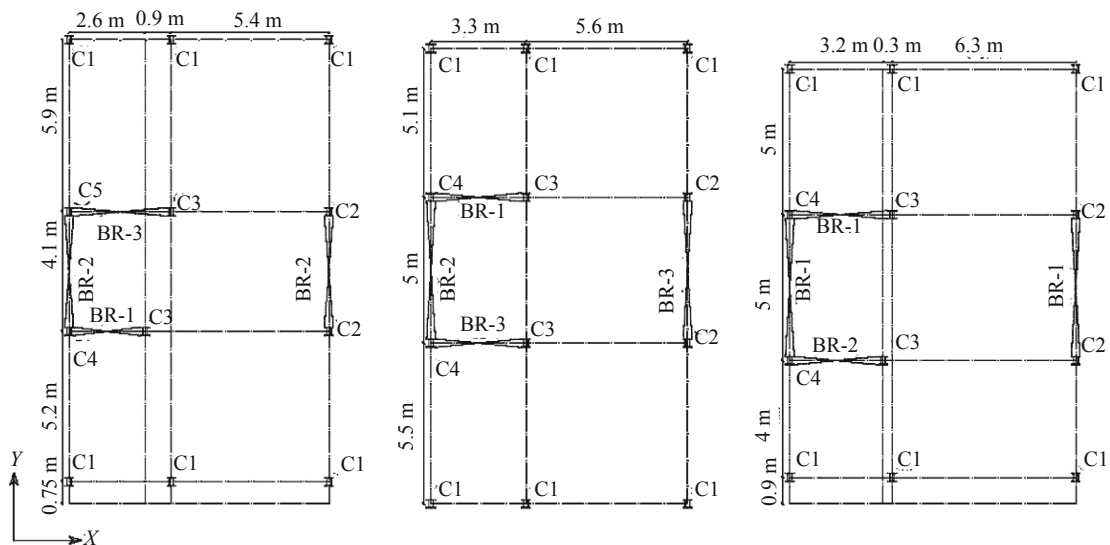


Fig. 1 Plan of the three selected buildings, left to right 3SB, 4SB and 5SB structure, respectively

Table 1 Specifications of the three selected buildings

Code	No. of storys	Area of floor (m ²)	Height (m)	Length of bracing-bay		$W_{(Total)}$ (t)	I_m (t·m ²)	T_1 (s)	T_2 (s)
				X (m)	Y (m)				
3SB	3	145	10.00	8.2	6.0	420	12100	0.62	0.49
4SB	4	149	13.30	10.0	6.5	614	18550	0.74	0.56
5SB	5	150	16.70	10.0	6.7	738	20960	0.89	0.61

Table 2 Characteristic sections of the three selected buildings (based on European standard)

		Story-1	Story-2	Story-3	Story-4	Story-5
5SB	C-1*	3I14+P10*0.8**	3I14****	2I14c/c***	2I14c/c	2I14c/c
	C-2	3I16+P28*1.2	3I16+P20*1.2	2I16+P20*0.6	2I16c/c	2I16c/c
	C-3	3I22+P28*1.0	3I22+P20*1	2I22+P20*0.6	2I22c/c	2I22c/c
	C-4	3I22+P28*1.8	3I22+P20*1.2	2I22+P20*0.6	2I22+P20*0.6	2I22c/c
	Br-1*	2U14**	2U12	2U12	2U10	2U10
	Br-2	2U16	2U12	2U10	2U10	2U10
4SB	C-1	2I14+P10*0.6	2I14c/c	2I14c/c	2I14c/c	
	C-2	3I14+P25*1	3I14+P10*0.6	3I14	2I14c/c	
	C-3	3I16+P28*1.2	3I16+P20*1.2	3I16	2I16c/c	
	C-4	3I14+P25*1.2	3I14+P10*1.2	2I14c/c	2I14c/c	
	Br-1	2U12	2U12	2U8	2U8	
	Br-2	2U10	2U10	2U8	2U8	
3SB	Br-3	2U12	2U10	2U8	2U8	
	C-1	2I14c/c	2I14c/c	2I14c/c		
	C-2	2I14+P12*1	2I14	2I14		
	C-3	2I18+P24*0.8	2I18+P24*0.8	2I18		
	C-4	2I18+P14*1	2I18+P14*0.8	2I18		
	C-5	2I16+P20*1	2I16+P12*0.6	2I16		
3SB	Br-1	2U10	2U10	2U8		
	Br-2	2U8	2U8	2U8		
	Br-3	2U12	2U10	2U8		

* C, Br show column and bracing elements, respectively.

** I, P and U show IPE section, column plates and UNP section, respectively and dimensions are in cm.

*** c/c show the batten-column with 14 cm distance of center to center.

**** triple I-sections.

tests were used. In order to calibrate the plastic behavior of the braced frames and the batten-columns, several parameters, such as the hysteretic behavior of the materials, were investigated in the mathematical model. For accurate modelling, the parameters were verified based on existing experimental results obtained by Fell *et al.* (2010), as well as by Jafari and Hashemi (2008). Two samples of the experimental tests were compared to the OpenSees results; they are shown in Fig. 2. Figure 2(a) relates to a batten column, whereas Fig. 2(b) refers to box section bracing, both of which are common in the current practice in Iran. The geometrical specifications and material properties determined by tests are reported in Table 3. There are some small differences between the analytical hysteretic loops and those obtained experimentally, and a very good match can be seen in Fig. 2.

2.3 Software modelling

The structures were modelled and analyzed using the OpenSees platform (2007) in three-dimensions. The characteristics of the models were as followings: (1) irregularly-shaped structural designs which result in non-uniform stiffness in plan; (2) the masses are lumped at the floor levels, where the horizontal degrees of freedom are defined; (3) the effect of nonstructural elements is neglected; (4) the partition walls consisted of lightweight blocks with weak connections to the steel frames (so that the effect of infill walls was not taken into account); (5) the one-way concrete slab has a thickness of only 0.1 m, and is reinforced with mesh reinforcement (F8@200 mm). Since load-bearing shear connectors were not sufficiently used, the

steel beams and concrete slab do not act perfectly as a composite structure, especially at the beam supports. It was therefore assumed that the floor diaphragms have adequate rigidity only in-plane so that the rotation of the columns was not restrained by these thin slabs; (6) the bracing members are welded to 1 cm thick gusset plates (this mean that no design thickness was adopted for the gusset plates in the designed existing buildings); (7) based on the test results, the steel tensile strengths ranged between 243.3 and 270.3 MPa, with a mean of 256.8 MPa; (8) the effect of the gusset plates and of the out-of-plane imperfection at the mid-point of the braces for initial camber is also taken into consideration; (9) the differences between the applied dead loads and the design loads were obtained from the field data; (10) a critical damping ratio of $\xi = 0.02$ is attributed to all of the vibration modes. For practical purposes, the first and third modes can be selected as providing reasonable values for the damping ratio in all the modes contributing significantly to the response (Chopra, 2012; Karamanci and Lignos, 2014). For this reason, in this study, the constants α and β were calculated based on these two modes as Rayleigh damping; (11) since all the beam end connections within the structures are pinned (with the use of perfectly flexible supported beams using a welded angle seat and a top welded angle), the beams are modelled by elastic elements; (12) the columns, bracings and gusset plates are modelled by nonlinear beam-column elements, the P-delta effects being taken into account (as was proposed by Uriz *et al.*, 2008); (13) five integration points were assigned to each brace as well as to the column; (14) the material response of the brace steel was represented by the Menegotto–Pinto material model with the kinematics and isotropic

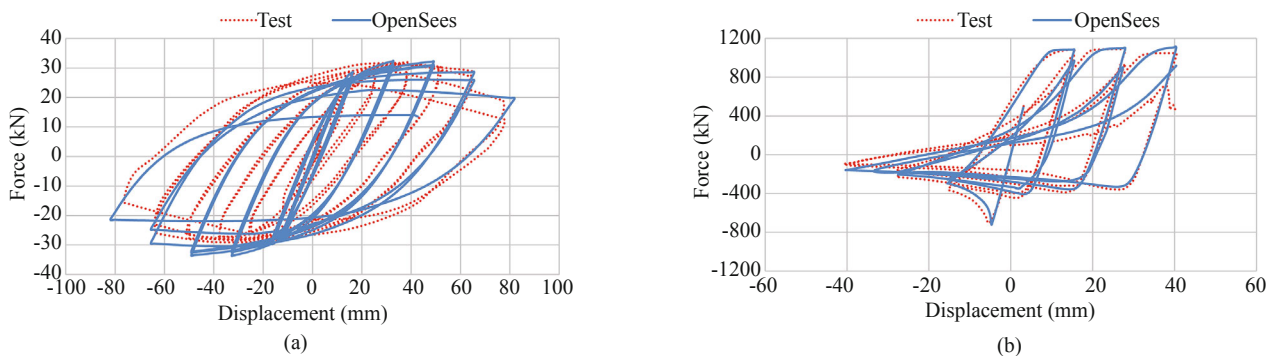


Fig. 2 Comparison of the material modelling and the test results: (a) batten column (Jafari and Hashemi, 2008), (b) Hss brace (Fell *et al.*, 2010)

Table 3 Geometrical specifications and material properties determined by tests

	Test	Section	σ_y (MPa)	Length (m)	Cyclic load protocol	Axial force (kN)
1	Jafari	2IPE100 (c/c120)*	254	1.20	ECCS (3 repetitions), ATC24	75
2	Fell	HSS100x100x0.64	320	2.75	Standard (2 repetitions), SAC/AISC	-

* The center-to-center distance 2IPE100 was equal to 120 mm

hardening that is available in OpenSees, using Steel02 material behavior. The strain hardening ratio was assumed to be 3%; (15) low cycle fatigue effects for all of the nonlinear elements was taken into account and the required parameters was taken from Uriz *et al.* (2008). Therefore, it used to properly capture the deterioration of the system; (16) corotational theory was used to represent the moderate to large deformation effects of inelastic buckling of the braces, and (17) fiber elements with continuous plasticity are used in all the nonlinear elements. Thus, twelve layers along the depth and width, and three layers across the thickness of the cross section, were defined.

3 Site hazard characterization

In this research, disaggregation analysis was performed in order to determine the target M , R , and ε values at probabilities of exceedance of 50%, 10% and 2% over a 50-year return period for Mashhad city's central area (site-Lat.: 36.286 and site-Long.: 59.616). The sample disaggregation results are presented in Table 4 and in Fig. 3, for three different hazard levels. Since the final disaggregation results corresponding to the first mode period are the same for each sample (3SB, 4SB and 5SB), they were drawn just at $T_1 = 0.89$ in Fig. 3. At each of the given hazard levels, the disaggregation results revealed different target ε values. For a high hazard level (assuming a return period of 2475 years), the hazard was dominated by $+2.5 < \varepsilon < +3.0$, whereas for a low hazard level (assuming a return period of 72 years), it was limited to the range: -0.5 to 0 . Thus, for each hazard level, independent sets of acceleration histories were selected based on the target ε values. Note that the target η value can be taken as being equal to the target ε , which refers to a linear combination of ε_{Sa} and ε_{PGV} .

4 Ground motion database / selection

The $M6.5$ SGM database proposed by Hatefi (2010), which was developed and processed for the reliable implementation of nonlinear dynamic analysis, was used to provide input for the development of the fragility curves. The effectiveness of SGMR's was investigated by Hatefi. The SGM database, which is given in Appendix (Table A), contains a bin of potential damaging scenario earthquakes in Iran with $6.0 < M < 7.6$, $PGA > 0.1$ g, $20 \text{ km} < R < 100 \text{ km}$, recorded on soil types II and III (similar to the C and D site classification given in NEHRP2000), which are the common soil types at the site. This set of SGM data is quite compatible with the specifications of the ground motion such as probable M and R events from source-to-site results and results concerning the faulting mechanism of the area. Finally, the following ε and η based values were used to select representative SGMR's as the input SGM time histories.

4.1 Epsilon-based record selection

The first method used in the current study was based on the records which have Epsilons that are compatible with the target ε of the ground motion disaggregation in the specified scenarios of different hazard levels at the site. For each sample, the ε values of the ground motion at T_1 (the first mode period) are derived, so that ε is defined as a measure of the difference between the spectral acceleration of a ground motion record and the mean value obtained from an attenuation prediction equation (the mean of Campbell and Bozorgnia 2003 and 2008 attenuation relations). Since the disaggregation results reflect the expectation: $(-0.5-0.0)$, $(+1.5-+2.0)$ and $(+2.5-+3.0)$ for return periods of 72, 475 and 2475

Table 4 Disaggregation results for a central location in Mashhad City

Return period (years)		72	475	2475
1	M	4.5–5.0	5.0–5.5	6.0–6.5
2	R (km)	0–10	0–10	0–10
3	ε and η	-0.5 to 0	+1.5 to +2.0	+2.5 to +3.0

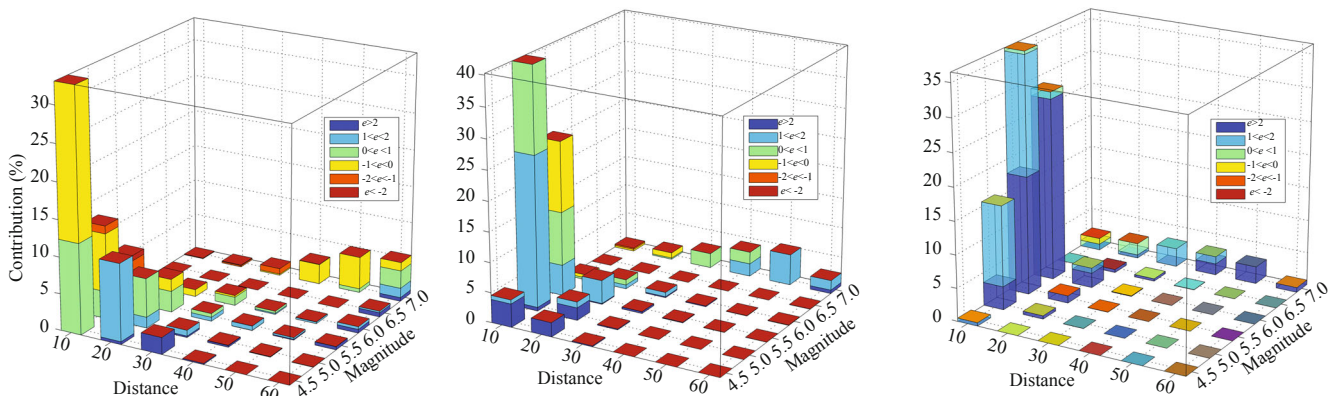


Fig. 3 A sample of hazard disaggregation results for return periods of (a) 72, (b) 475 and (c) 2475 years at $T = 0.89$ s

years, respectively, the database records were classified according to the predicted ε at T_1 .

4.2 Eta-based record selection

Mousavi *et al.* (2011) introduced the parameter η as an alternative indicator of spectral shape, which results in a more reliable prediction of the nonlinear response. They showed that the parameter η , as a linear combination of ε_{Sa} and ε_{PGV} , was significantly more efficient than the well-known and convenient parameter ε_{Sa} . In the following section, it is shown that η -based intensity measures can be used to decrease bias in structural performance assessments, as well as to increase the efficiency of structural response prediction (which can lead to a reduction in the number of dynamic analyses required to estimate response with a given precision).

The parameter η was introduced as:

$$\eta = 0.485 + 2.454 \varepsilon_{Sa} - 2.020 \varepsilon_{PGV} \quad (1)$$

In order to obtain better estimates, the calculations were repeated and the coefficients were verified based on the applied data set. Consequently, a new expression for η was derived in this study.

Standard hazard disaggregation analysis can provide values of the target ε_{Sa} but not of the target ε_{PGV} . However, similar values for Epsilons can be challenged since different Epsilons may not be equal to the different hazard levels. For this reason, the correlation between ε_{Sa} and ε_{PGV} values corresponding to different periods was studied herein (Azarbakht *et al.*, 2014). A linear regression is first implemented in order to evaluate the target ε_{PGV} for a given ε_{Sa} . The results were derived empirically from the above-mentioned SGM database and from the different values of ε associated with the desired range of periods, from 0.2 to 1.2 s (i.e. a wider range of first mode periods of structures was taken into account). Figure 4 shows ε_{PGV} versus ε_{Sa} for the 7070 data points. As expected, it was found that a direct relation exists between these Epsilons (ε_{PGV} and ε_{Sa}). It can be defined by Eq. (2) as:

$$\varepsilon_{PGV} = c_0 + c_1 \cdot \varepsilon_{Sa}, \quad c_0 = 0.431, c_1 = 0.861 \quad (2)$$

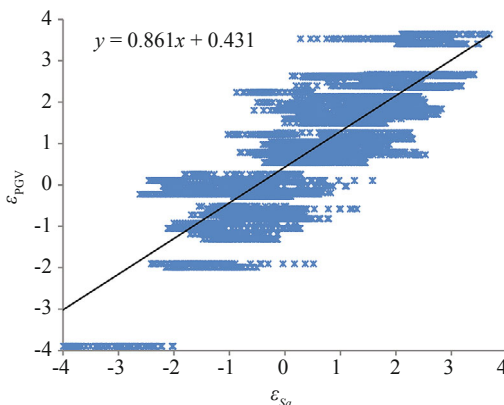


Fig. 4 Relation between ε_{PGV} and ε_{Sa}

Now, if it is assumed that the target η value is equal to the target ε_{Sa} value; the final form of the parameter η is:

$$\eta = 1.217 + 3.432\varepsilon_{Sa} - 2.824\varepsilon_{PGV} \quad (3)$$

The target η is thus obtained from the disaggregation analysis as being equal to the target ε defined in Table 4 in the last section, the η -based record selection being carried out based on Eq. (3). In order to validate this equation, the mean damage at the CP level was calculated using both the η -filtration and the ε_{Sa} -filtration procedures. Figures 5 and 6 show the coefficient of correlation between the parameters ε_{Sa} and η for the three typical structural models. These figures show that the parameter η is a better predictor of damage, with an average 35% improvement in the coefficient of correlation, and the sufficiency of the response increases with the damage level (where R is the normalized response).

On the other hand, an efficient IM is defined as one that results in a relatively small variability of the structural response for a given IM level. Figure 7 indicates that the response dispersion is substantially reduced in most cases when η is used instead of ε , which implies that the number of records needed to achieve the same estimated accuracy is reduced. Thus, this spectral shape parameter increases the efficiency of the response predictions when using the η parameter as the IM.

The final desirable IM property is the scaling records to a value of the IM results in the unbiased structural responses. This property is scaling robustness, which represents sufficiency with respect to scale factor when the records are linearly scaled to perform structural analyses. Table 5 shows that scaling the records to ε tends to result in biased structural responses, which increase as the scale factors increase. On the other hand, when using η , there is no statistically significant trend between the maximum inter-story drift ratio (MIDR) and the logarithm of the scale factor, indicating that η -based values are a more robust predictor of damage with respect to scaling than ε -based values. It is therefore reasonable to use η as a new index for predicting nonlinear response versus ε in the case of irregular multi-story buildings.

5 Nonlinear dynamic analyses

Nonlinear IDA, using $S_a(T_1)$ as the IM, was performed in the case of all three of the above-mentioned models, and the intensity of $S_a(T_1)$ was increased incrementally until a particular limit state was reached (Vamvatsikos *et al.*, 2003). Thus, both of the horizontal components of the ground motion were used for the IDA analysis, and the results were obtained for the selected SGMR's based on ε and η . For each structure, the analyses were performed in batches of 420, corresponding to the 12 levels of appropriately scaled IM for all 35 records.

Based on the assumptions of existing methodologies, failure was defined by two different methods: (1) the IDA curve may become a flat line, which means that

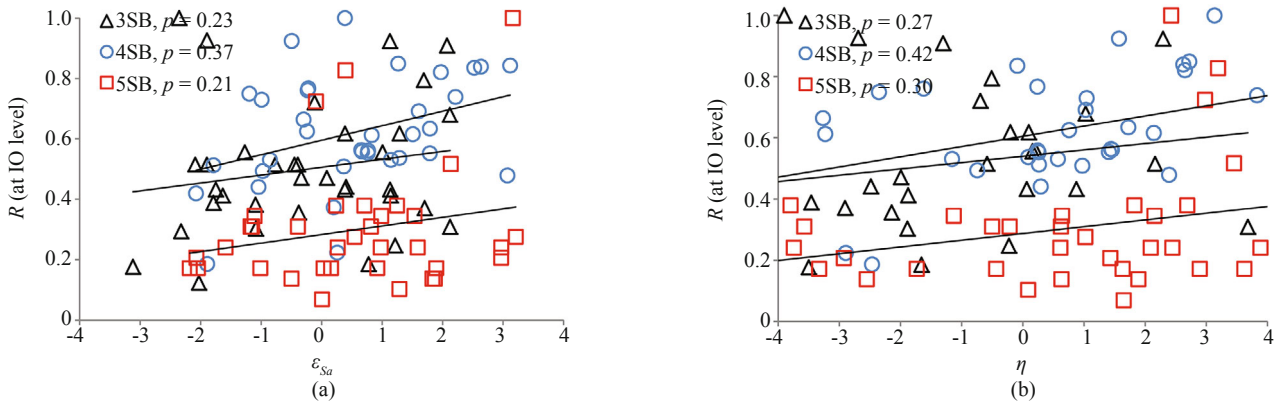


Fig. 5 Improvement in the coefficient of correlation between the response predictors and damage for samples at the immediate occupancy (IO) level, (a) ϵ_{Sa} , (b) η

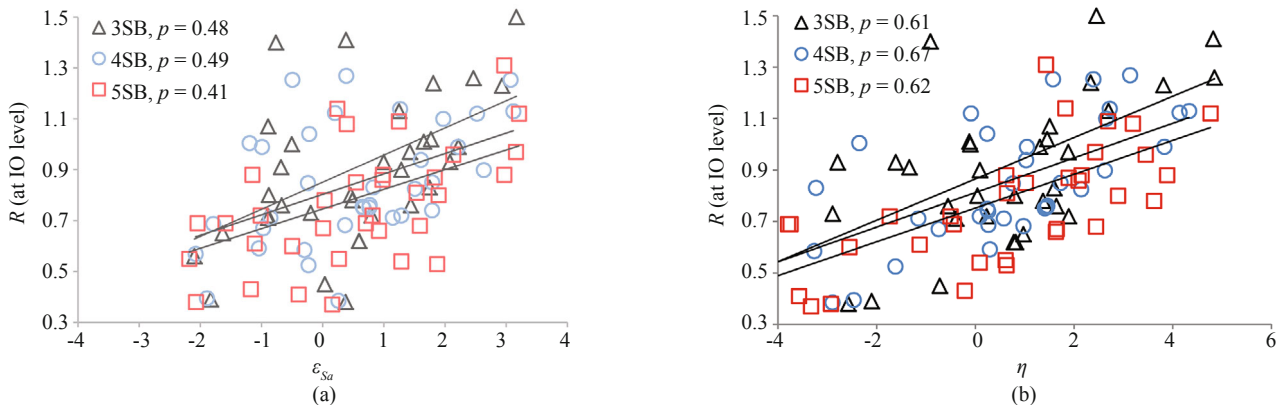


Fig. 6 Improvement in the coefficient of correlation between the response predictors and damage for samples at the collapse prevention (CP) level, (a) ϵ_{Sa} , (b) η

Table 5 Comparison of the correlation of MIDR to the scale factor for the scale of the records

IM Parameter		72	475	2475
1	ϵ -based	0.367	0.162	0.126
2	η -based	0.081	0.083	0.063

the solution has not converged completely, or (2) the rate of decrease in stiffness with increasing record intensity exceeds a prescribed MIDR, and is considered doubtful beyond 10% (Cornell *et al.*, 2005). For this reason, $c_1 = 0.861$ the time histories for the horizontal displacement were, in the case of the braced frames, reported as Engineering Demand Parameters (EDP), as defined in the OpenSees output. Figure 8 shows the IDA curves of all samples.

6 Proposed fragility curve

6.1 Damage calculation method

Except in the case of a few brittle systems and acceleration-sensitive elements, building damage can be primarily expressed as a function of a building's relative displacements. Furthermore, in order to

illustrate the overall structural response, and to achieve greater accuracy in the seismic assessment of irregular structures, a damage index should be able to reflect three-dimensional structural behavior, such as torsion. The simplest technique for combining local damage indices is to use a weighing scheme. The use of a weighted average procedure to calculate the global damage index can properly account for the local concentration of damage, distinguishing between low and high damage levels. The procedure applied in this study, for the damage assessment of structures with planar irregularities, was

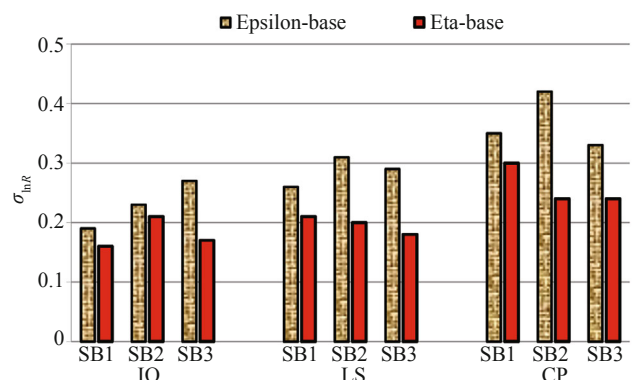


Fig. 7 Comparison of effectiveness of IM (standard deviation) with ϵ_{Sa} and η -based record selection

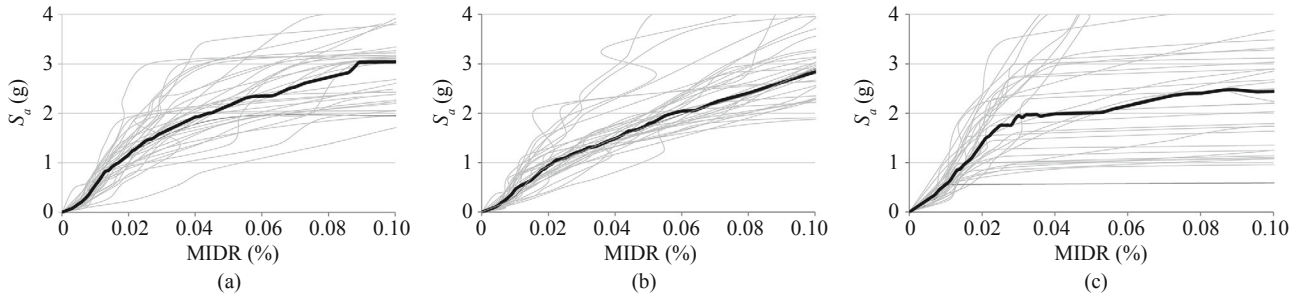


Fig. 8 IDA curves: (a) 3SB, (b) 4SB and (c) 5SB

proposed by Jeong and Elnashai (2006), but it does have the following modest shortcomings: (1) local collapse does not indicate overall collapse, and (2) the methodology was established for single-story irregular buildings. For this reason, the method was improved within the scope of this study, and applied to multi-story irregular structures.

The proposed method makes three important assumptions that are generally used in formulating weighted average damage indices. These assumptions involve: (1) the placing of emphasis on severely damaged local elements; (2) the use of gravity loads supported by each local component for its weighting factor; and (3) the assumption that the overall damage index increases as the local damage level increases. This means that the importance of each frame relative to the total building damage is a function of the frame damage level.

The modified procedure is summarized in the following steps: (1) the damage to individual braced frames is determined from the transient drift ratio of the 3D model for each frame. Here, the structural drift limit states (e.g. IO, LS and CP levels) of a planar braced frame based on FEMA-356 are defined. The FEMA approach was used to define inter-story drifts of 0.005, 0.015 and 0.02 as the typical values, which correspond to the previously mentioned structural performance levels; (2) the influencing area (effective gravity loads) of each frame was calculated; (3) the influencing area (as the weighted ratio) was modified based on a linear relation according to the local damage level. The weighting factor could also depend on the magnitude of the damage index of the frame, so that severely damaged frames are weighted more heavily; (4) the story damage index is obtained as a weighted average of the local damage indices of all the braced frames at each story level in a given direction, using Eq. (8). The maximum of the damage indices for the critical direction x or y is then selected for each story (D_{gn}); and (5) overall, the damage index of the structure is obtained by a weighted summation of the story damage indices on the basis of the hysteretic energy in each story in Eq. (9).

Based on the above assumptions, the damage index was defined as follows:

$$W_{j,c} = W_{j,max} - W_j \quad (4)$$

$$W_{F1} = W_1 - D_j \cdot W_{j,c} \quad (5)$$

$$W_{Fj} = W_j + D_j \cdot W_{j,c} \quad (6)$$

$$D_{gxn} = (W_{F1} \times D_1 + W_{Fj} \times D_j) / W_t \quad (7)$$

$$D_{gxn} = \sum_{i=1}^m D_i \cdot W_i / W_t + \sum_{i=1}^m \left\{ W_i / W_t \cdot [D_j^2 - D_i \cdot D_j] \right\} \quad (8)$$

where D_{gxn} is the x -global damage index in story n , D_j is the local damage index of the critical braced frame in story n (D_{max}), D_i is the local damage index of the braced frame i , W_t is the total effective weight in story n , W_i is the attributed gravity weight of the braced frame i in story n , and m is the number of braced frames in the x direction.

$$D_g = \sum_{n=1}^N D_{gn} \cdot E_n / E_t + \sum_{n=1}^N \left\{ E_n / E_t \cdot [D_{gmax}^2 - D_{gmax} \cdot D_{gxn}] \right\} \quad (9)$$

where: D_g is the overall damage index, E_i is the hysteretic energy of story i , E_t is the total hysteretic energy, D_{gn} is the maximum of D_{gxn} and D_{gyn} for story n , D_{gmax} is the maximum of D_{gn} in the multi-story building, and N is the number of stories.

Figure 9 shows the assessment results at the three selected structural limit states (IO, LS or CP) for the three damage indices. The damage indices were derived based on the maximum drift at the center of mass, the maximum drifts at the most critical point of the building, and the proposed method. In most cases, lower values for the proposed index are shown, as can be seen in Fig. 9. Since, in the case of 3D response, the effect of torsion is significant, the damage states estimated by the proposed index are often significantly higher than those estimated from the calculated drift at the center of mass. On the other hand, since the damage was determined based on the drift ratio for each frame, measurements at critical points (the most critical point is at the corner of the building) are more conservative for damage assessment.

6.2 Modelling uncertainty

Modelling uncertainty can have a significant impact on the assessed risk of earthquake-induced damage and collapse in a building obtained through the PBE framework. In the damage assessment of a building, two main sources of uncertainty are present: (a) uncertainty

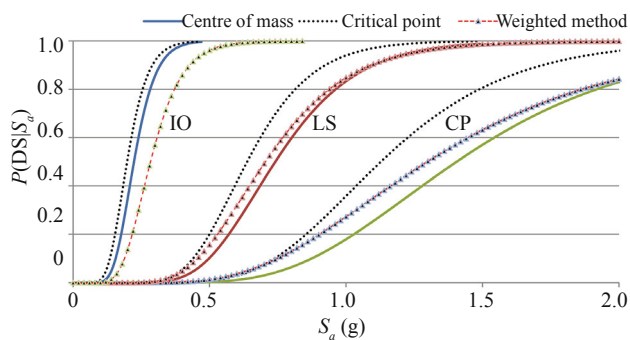


Fig. 9 Comparison of the fragility curves corresponding to the three damage indices

due to the selected ground motions used in the analysis, known as record-to-record (RTR) uncertainty. Here, RTR uncertainty is incorporated through the development of a robust technique for ground motion selection by η as well as IDA, and (b) uncertainty embedded in the simulation model, known as modelling uncertainty.

Modelling uncertainty originates in the variation of the physical properties of building components, as well as in the variation of the representation of these properties in an analytical model. Variation of the different modelling parameters was taken into account in order to quantify the significance of modelling uncertainty using the FOSM method (Baker and Cornell, 2003; Haselton and Deierlein, 2007). Randomness was modelled by random variables based on field and test data such as steel yield/ultimate strength, construction error, additional dead loads and modulus of elasticity, as shown in Table 6. The 10th and 90th percentiles of the Gaussian distribution, as the lower and upper bounds of the random variables, were taken into account. On this basis, the dispersion of results was calculated from the fragility curves. The results showed that incorporating modelling uncertainty leads to an increase in the dispersion of the fragility curves by 8% to 20%, as shown in Table 7. These values increase as the number of stories increase, as well as with the damage level. Also, it appears that the level of nonlinearity increasingly affects the variability of the observed parameters.

7 Fragility curve results

Here the structural damage fragility curves are defined as the weighted drift ratios which define the thresholds of different damage states versus the spectral acceleration at a specified hazard level. Using the SGM indices, S_{a^o} and the damage ratio, median values of the

fragility curves were constructed, and the cumulative probability of the occurrence of damage was assumed to be lognormal as (Aslani and Miranda, 2003):

$$F = P(d > D_i | IM) \quad (10)$$

where F is the fragility function, P is a probability function; d denotes the damage level of the structure, D_i represents the i th damage state, and IM denotes the ground motion intensity parameter (S_a) and ($i = 1$ to n) shows the different damage states.

Figures 10(a), (b) and (c) show comparisons of the fragility curves corresponding to the typical structures versus the type of SGMR selection. These curves are derived from the scatter of points using the least squares method. It can be seen that the ε -based and η -based SGMR selections can give good estimates of the median damage capacity in comparison with the use of all of the records. It is higher for the 475 and 2475 year return periods, and slightly lower for the return period of 72 years, when the record selection takes into account the ε and η values, respectively. It was observed that the differences in the fragility curves increase steeply with increasing ε and η values, as well as with the site hazard levels. These results demonstrate the importance of ground motion selection criteria in accurately predicting building limit states. Similarly, Figures 10(a), (b) and (c) show that if ε is neglected in the simulations, the median predicted probability of collapse capacity is increased by less than 12% for a return period of 72 years, whereas it would be decreased by 23% and 32% in the case of return periods of 475 and 2475 years, respectively. Furthermore, it can be seen that the two different filtration approaches result in two distinct mean collapse capacities. The difference between the ε and η -filtrations is, in some cases, significant, whereas in other cases it is almost negligible. Figure 10(d) shows the change of the η -based record selection from the return period of 72 years to 2475 years reduces the probability of exceedance of the expected performance levels by less than 40%. As a result, the probability of a higher level of expected damage increases with the number of stories, from three to five. Table 8 shows the final fragility function parameters with η -based record selection at three hazard levels.

Figure 11 shows a comparison of the estimated probability of exceedance of the expected damage states for the typical steel braced buildings from the present study with the observed major earthquakes in Iran such as those of Manjil, Bam and Qaen (Ghodrati-Amiri

Table 6 Lower/upper levels of the random variables using 10th and 90th percentiles based on the field and test data

No.	Parameter	Mean	COV.	Lower-upper bound
1	Out-of-plane imperfection (% of the brace length)	0.0015	33%	0.0009–0.0021
2	IPE, UPA and plate yield strength (MPa)	256.8	4.1%	243.3–270.3
3	Additional construction dead load (%)	1.19	18.4%	0.764D–1.236D
4	Modulus of elasticity (MPa)	197000	7.0%	0.91E _s –1.09E _s

Table 7 Increase in the dispersion with consideration of modeling uncertainty

Model	IO	LS	CP
3SB	0.08	0.11	0.12
4SB	0.11	0.15	0.17
5SB	0.13	0.18	0.20

et al., 2007; Jalalian, 2006; Moghadam, 2005). From this figure it can be seen that the developed fragility curves are in relatively good agreement with the observed data corresponding to post-earthquake damage distribution, and the validity of these functions are therefore confirmed.

Table 8 Estimated fragility function parameters based on η record selection at three hazard levels

Building type	Damage state	50% in 50 Yrs		10% in 50 Yrs		2% in 50 Yrs	
		Mean	Log-St-Dev	Mean	Log-St-Dev	Mean	Log-St-Dev
3SB	IO	0.196	0.43	0.217	0.48	0.217	0.35
	LS	0.741	0.30	0.835	0.27	1.01	0.28
	CP	1.17	0.41	1.336	0.42	1.462	0.31
4SB	IO	0.082	0.45	0.122	0.49	0.135	0.40
	LS	0.533	0.417	1.768	0.39	0.631	0.50
	CP	0.771	0.53	1.00	0.47	1.105	0.53
5SB	IO	0.074	0.44	0.091	0.39	0.105	0.67
	LS	0.247	0.63	0.333	0.66	0.382	0.63
	CP	0.549	0.73	0.577	0.73	0.698	0.68

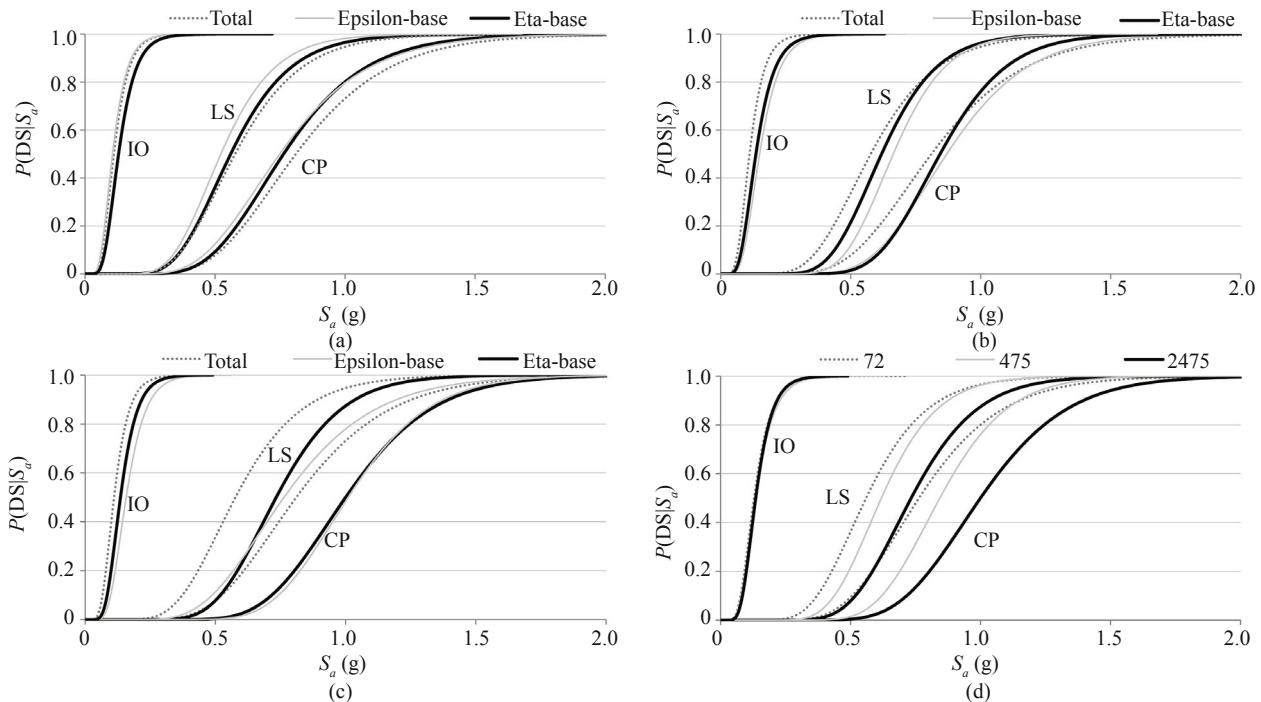


Fig. 10 Comparison of the fragility curves corresponding to 3 to 5 story structures: (a) 72 years, (b) 475 years and (c) 2475 years return period for the IO, LS and CP performance levels with and without consideration of Epsilon or Eta, and (d) The final fragility curves using Eta-based SGMR selection

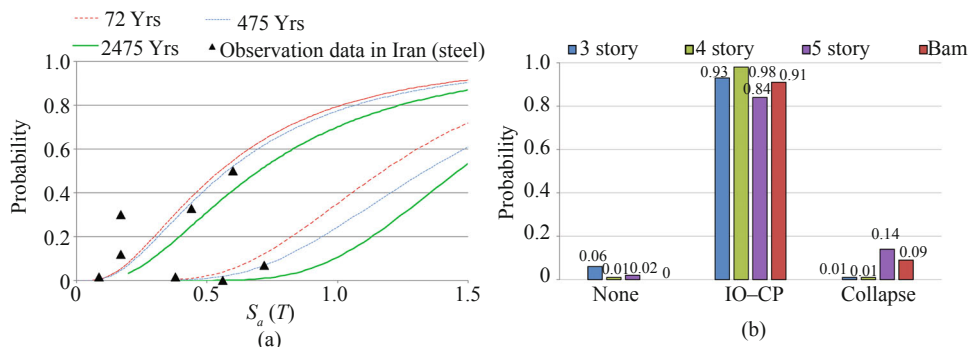


Fig. 11 Comparison of the probability of expected damage states in the present study with (a) the major earthquakes in Iran, and (b) the Bam earthquake

8 Conclusions

The drift-based fragility of typical existing steel-braced frame buildings has been investigated using a weighting approach for the calculation of potential damage to irregular buildings. Based on a comprehensive building taxonomy performed in Mashhad city, as a case study, three typical structural models were developed for nonlinear dynamic analysis. The distribution of the damage indices corresponding to each ground motion IM (S_a) was estimated by numerous incremental dynamic analyses.

Epsilon and Eta based methods were used for SGMR selection, and a disaggregation analysis was performed for the site. Also, the influence of the η -parameter as a linear combination of ε_{Sa} and ε_{PGV} in the SGMR selection, was investigated in order to obtain a more reliable collapse capacity assessment. It is shown that η -based SGMR's selection is more efficient, sufficient and robust than ε -based SGMR's selection. Also, based on the results of the regression analysis, an equation was proposed to predict the target ε_{PGV} based at a given ε_{Sa} .

The results showed that a change in the ε and η based record selection decreases the probability of exceedance of the expected performance levels. Also, at some hazard levels, the difference in the collapse capacity of structures resulting from η and ε filtration is very significant. It seems that, at high hazard levels, the investigated typical steel braced frame buildings are safe against collapse at the site. The resulting fragility curves for these structures were often found to be lower in the case of η -based record selection, compared with the ε_{Sa} -based record selection. The developed fragility curves are in relatively good agreement with the observed earthquake data using weighted damage indices.

References

- Aslani H and Miranda E (2003), "Probabilistic Assessment of Building Response during Earthquakes," *Proc. Ninth International Conference on Application of Statistics and Probability in Civil Engineering*, San Francisco, CA, **2**: 1441–8.
- AzARBakht A, Mousavi M, Nourizadeh M and Shahri M (2014), "Dependence of Correlations between Spectral Accelerations at Multiple Periods on Magnitude and Distance," *Earthquake Engineering & Structural Dynamics*, **43**(8): 1193–1204.
- AzARBakht A, Shahri M and Mousavi M (2015), "Reliable Estimation of the Mean Annual Frequency of Collapse by Considering Ground Motion Spectral Shape Effects," *Bulletin of Earthquake Engineering*, **13**(3): 777–797.
- Baker JW and Cornell CA (2003), "Uncertainty Specification and Propagation for Loss Estimation Using FOSM Methods," *PEER Report 2003/07*, Pacific Earthquake Engineering Research Centre, University of California, Berkeley, CA.
- Baker JW and Cornell CA (2006), "Spectral Shape, Epsilon and Record Selection," *Earthquake Engineering & Structural Dynamics*, **34**(10): 1193–1217.
- Benavent-Climent A (2007), "An Energy-based Damage Model for Seismic Response of Steel Structures," *Earthquake Engineering and Structural Dynamics*, **36**: 1049–1064.
- Bojórquez E, Iervolino I, Reyes-Salazar A and Ruiz SE (2012), "Comparing Vector-valued Intensity Measures for Fragility Analysis of Steel Frames in the Case of Narrow-band Ground Motions," *Engineering Structures*, **45**: 472–480.
- Building and Housing Research Center (1999), *Iranian Code of Practice for Seismic Resistant Design of Buildings*, (Standard No.2800, 2nd edition), Tehran, Iran.
- Chopra AK (2012), *Dynamics of Structures: Theory and Applications to Earthquake Engineering*, 4th Edition, Prentice Hall, Englewood Cliffs, New Jersey.
- Cornell A, Zareian F, Krawinkler H and Miranda E (2005), "Prediction of Probability of Collapse," In *H. Krawinkler (Ed.), Van Nuys Hotel Building Testbed Report: Exercising Seismic Performance Assessment*, Pacific Earthquake Engineering Research, 4.5.Vol. 2005/11: 85–93.
- Eads L, Miranda E and Lignos DG (2015), "Average Spectral Acceleration as an Intensity Measure for Collapse Risk Assessment," *Earthquake Engineering and Structural Dynamic*, **44**(12): 2057–2073.
- Estekanchi H and Arjomandi K (2007), "Comparison of Damage Indexes in Nonlinear Time History Analysis of Steel Moment Frames," *Asian Journal of Civil Engineering*, **8**(6): 629–646.
- Fell BV, Kanvinde AM and Deierlein GG (2010), "Large-scale Testing and Simulation of Earthquake Induced Ultra Low Cycle Fatigue in Bracing Members Subjected to Cyclic Inelastic Buckling," *Technical Report #172*, Blume Earthquake Engineering Center, Stanford University, Stanford, CA.
- FEMA-356 (1997), *NEHRP Prestandard and Commentary for the Seismic Rehabilitation of Buildings*, Federal Emergency Management Agency, Washington, D.C.
- Gerami M, Sharbati Y and Sivandi-Pour A (2013), "Nonlinear Seismic Vulnerability Evaluation of Irregular Steel Buildings with Cumulative Damage Indices," *International Journal of Advanced Structural Engineering*, **5**(1): 1–15.
- Ghobarah H, Abou-Elfath H and Biddah A (1999), "Response-based Damage Assessment of Structures," *Earthquake Engineering and Structural Dynamic*, **28**: 79–104.
- Ghodrati Amiri G, Jalalian M and Razavian Amrei SA (2007), "Derivation of Vulnerability Functions Based on Observational Data for Iran," *Proceedings of the International Symposium on Innovation & Sustainability*

- of Structures in Civil Engineering, Shanghai, China.
- Gehl P, Seyedi DM and Douglas J (2013), "Vector-valued Fragility Functions for Seismic Risk Evaluation," *Bulletin of Earthquake Engineering*, **11**(2): 365–384.
- Goulet C, Haselton CB, Mitrani-Reiser J, Stewart JP, Taciroglu E and Deierlein G (2006), "Evaluation of the Seismic Performance of a Code-conforming Reinforced Concrete Frame Building - Part I," Paper NCEE-1576, *Proc. 8th National Conference on Earthquake Engineering*, San Francisco, CA.
- Haselton CB and Deierlein GG (2007), "Assessing Seismic Collapse Safety of Modern Reinforced Concrete Frame Buildings," *PEER Report 2007/08*, Pacific Earthquake Engineering Research Center, University of California, Berkeley, CA.
- Hatefi H (2010), "Nonlinear Dynamic Analysis Based on M6.5 Strong Ground Motion Database," *MSc Dissertation*, Dept. of Civil Engineering, IIEES, Tehran, Iran.
- Jafari MA and Hashemi HB (2008), "Experimental Investigation on Seismic Behaviour of Batten Columns," *PhD. Dissertation*, International Institute of Earthquake Engineering and Seismology (IIEES), Tehran, Iran.
- Jalalian M (2006), "Deriving of Empirical Vulnerability Functions for Iran," *MSc Dissertation*, University of Technology, Tehran, Iran.
- Jeong SH and Elnashai AS (2006), "New Three Dimensional Damage Index for RC Buildings with Plan Irregularities," *Journal of Structural Engineering (ASCE)*, **132**(9):1482–1490.
- Karamanci E and Lignos DG (2014), "Computational Approach for Collapse Assessment of Concentrically Braced Frames in Seismic Regions," *Journal of Structural Engineering*, A4014019.
- Khashae P (2005), "Damage-based Seismic Design of Structures," *Earthquake Spectra*, **21**: 371–387.
- Lu X, Ye L, Lu X, Li M and Ma X (2013), "An Improved Ground Motion Intensity Measure for Super High-rise Buildings," *Science China Technological Sciences*, **56**(6): 1525–1533.
- Moghadam AS (2005), "Ground-based Damage Statistics of Buildings that Survived the 2003 Bam, Iran," *Earthquake Spectra*, **21**(S1): S425–37.
- Mousavi M, Ghafory-Ashtiany M and Azarbakht A (2011), "A New Indicator of Elastic Spectral Shape for the Reliable Selection of Ground Motion Records," *Earthquake Engineering & Structural Dynamics*, **40**(12):1403–1416.
- OpenSees (2007), *Open System for Earthquake Engineering Simulation Manual*, Pacific Earthquake Engineering Research Center, University of California, Berkeley, CA.
- Shirian F (2005), "Seismic Rehabilitation of Existing Steel Braced Frames to Achieve Current Seismic Regulations," *MSc Dissertation*, Department of Civil Eng, Kharazmi University, Tehran, Iran.
- Uriz P, Filippou FC and Mahin SA (2008), "Model for Cyclic Inelastic Buckling for Steel Member," *Journal of Structural Engineering*, ASCE, **134**(4): 619–628.
- Vamvatsikos D, Jalayer F and Cornell CA (2003), "Application of Incremental Dynamic Analysis to an RC Structure," *Proceedings of the Conference: FIB Symposium*, Concrete Structures in Seismic Regions, Athens, Greece.
- Williams MS and Sexsmith RG (1995), "Seismic Damage Indices for Concrete Structures: a State-of-the-art Review," *Earthquake Spectra*, **11**(2): 319–349.
- Yakhchalian M, Amiri GG and Nicknam A (2014), "A New Proxy for Ground Motion Selection in Seismic Collapse Assessment of Tall Buildings," *The Structural Design of Tall and Special Buildings*, **23**: 1275–1293.
- Yakhchalian M, Nicknam A and Amiri GG (2015), "Optimal Vector-valued Intensity Measure for Seismic Collapse Assessment of Structures," *Earthquake Engineering & Engineering Vibration*, **14**(1): 37–54.

Appendix

Table A Details of 35 earthquake ground motions considered in this study

No	Event	Year	Station	M_w	PGA (g)	R (km)	V_{s3} (m/s ²)
1	Bandar-abbas	1975	Bandar-Abbas	6.1	0.13	36	337
2	Tabas	1978	Boshrooye	7.4	0.10	55	564
3	Tabas	1978	Tabas	7.4	0.81	54	645
4	Tularud	1978	Talesh	6.0	0.24	15	539
5	Qaen	1979	Khezri	7.1	0.10	75	701
6	Qaen	1979	Gonabad	7.1	0.10	93	529
7	Golbaft	1981	Golbaft	7.0	0.28	13	365
8	Manjil	1990	Qazvin	7.4	0.27	94	456
9	Manjil	1990	Abhar	7.4	0.21	101	291
10	Manjil	1990	Ab-bar	7.4	0.57	41	291
11	Eslam-abad	1997	Kariq	6.0	0.57	48	589
12	Avaj	2002	Kaboodar-A	6.5	0.16	62	613
13	Avaj	2002	Razan	6.5	0.20	35	314
14	Firoozabad	2004	Hasan-Keyf	6.3	0.84	42	339
15	Firoozabad	2004	Moalem-Kel	6.3	0.29	99	490
16	Enchehborun	2005	Agh-Gala	6.1	0.12	14	341
17	Zarand	2005	Zarand	6.4	0.32	16	226
18	Erzurum	1983	Meteorologi-Ist	6.6	0.17	35	316
19	Adana	1998	Tarum-Ilce	6.2	0.28	48	263
20	Adana	1998	Meteorologi-Ist	6.2	0.13	65	366
21	Kokaeli	1999	Devlet-Has	7.4	0.14	81	348
22	Kokaeli	1999	Meteorologi-Ist	7.4	0.37	101	282
23	Kokaeli	1999	Marmara-Ara	7.4	0.12	43	701
24	Duzce	1999	Bayindirlik	7.1	0.81	36	294
25	Bingol	2003	BayindirlikIsk	6.3	0.50	12	529
26	Northridge	1994	Beverly-Hills	6.7	0.49	13	356
27	Northridge	1994	Can-country	6.7	0.48	27	309
28	Frioli	1976	Tolmezzo	6.5	0.34	20	425
29	San-Fernando	1971	La-Hollywood	6.6	0.18	40	316
30	Imp-Valley	1979	Delta	6.5	0.34	34	275
31	Landers	1992	Yermo-Fire	7.3	0.24	86	354
32	Loma-Prieta	1989	Hollister-C-Hall	6.9	0.25	47	199
33	New-Zealand	2010	Heathcote-V	7.0	0.63	43	-
34	Chi-Chi	1999	Chi-CHY101	7.6	0.40	32	259
35	Chi-Chi	1999	Chi-TCU045	7.6	0.47	76	701